Draft version January 12, 2013
Preprint typeset using LaTeX style emulateapj v. 11/10/09

arXiv:1102.1387v1 [astro-ph.SR] 7 Feb 2011

PERIODIC VARIABILITY OF LOW–MASS STARS IN SDSS STRIPE 82

A.C. Becker[1], J.J. Bochanski[2], S.L. Hawley[1], Ž Ivezić[1], A.F Kowalski[1], B. Sesar[1], A.A. West[3],

Draft version January 12, 2013

ABSTRACT

We present a catalog of periodic stellar variability in the “Stripe 82” region of the Sloan Digital Sky Survey (SDSS). After aggregating and re–calibrating catalog–level data from the survey, we ran a period–finding algorithm (Supersmoother) on all point–source lightcurves. We used color selection to identify systems that are likely to contain low–mass stars, in particular M dwarfs and white dwarfs. In total, we found 207 candidates, the vast majority of which appear to be in eclipsing binary systems. The catalog described in this paper includes 42 candidate M dwarf / white dwarf pairs, 4 white–dwarf pairs, 59 systems whose colors indicate they are composed of 2 M dwarfs and whose lightcurve shapes suggest they are in detached eclipsing binaries, and 28 M dwarf systems whose lightcurve shapes suggest they are in contact binaries. We find no detached systems with periods longer than 3 days, thus the majority of our sources are likely to have experienced orbital spin–up and enhanced magnetic activity. Indeed, twenty–six of twenty–seven M dwarf systems that we have spectra for show signs of chromospheric magnetic activity, far higher than the 24% seen in field stars of the same spectral type. We also find binaries composed of stars that bracket the expected boundary between partially and fully convective interiors, which will allow the measurement of the stellar mass–radius relationship across this transition. The majority of our contact systems have short orbital periods, with small variance (0.02 days) in the sample near the observed cutoff of 0.22 days. The accumulation of these stars at short orbital period suggests that the process of angular momentum loss, leading to period evolution, becomes less efficient at short periods. These short–period systems are in a novel regime for studying the effects of orbital spin–up and enhanced magnetic activity, which are thought to be the source of discrepancies between mass–radius predictions and measurements of these properties in eclipsing binaries.

Subject headings: binaries: eclipsing — stars: low-mass, brown dwarfs

1. INTRODUCTION

Over the last decade, advances in information technology have enabled larger and more ambitious astronomical surveys, which have provided more survey area, photometric depth, and wavelength coverage than in the cumulative history of astronomy. The largest surveys have imaged the entire observable sky, generally in multiple passbands but only for a single epoch. Other surveys imaged smaller portions of the sky repeatedly in order to resolve temporal variability in the Universe. Future surveys promise to merge both of these capabilities into broad synoptic surveys that will image the entirety of the available sky multiple times. The large etendue ($A\Omega$) and fast temporal resolution (10–15s) of next generation surveys will provide novel insights into the temporal behavior of the Universe, as well as more accurate colors for non–variable objects through repeat observations.

One forerunner to these next–generation surveys is the Sloan Digital Sky Survey (SDSS; York et al. 2000), a photometric and spectroscopic survey whose most recent data release (DR7; Abazajian et al. 2009) includes single–epoch imaging of approximately 10^4 square degrees. The flux densities of detected objects are measured almost simultaneously in five bands (u, g, r, i, and z; Fukugita et al. 1996) with effective wavelengths of 3551 Å, 4686 Å, 6166 Å, 7480 Å, and 8932 Å, 95% complete for point sources to limiting magnitudes of 22.0, 22.2, 22.2, 21.3, and 20.5 per exposure. The associated photometric catalogs contain brightness, color, shape, and positional information for more than 3×10^8 unique objects. These extensive data have enabled exciting investigations into the intrinsic properties of low–mass stars. The average colors (Hawley et al. 2002; West et al. 2005; Bochanski et al. 2007b; West et al. 2008), absolute magnitudes (Bochanski 2008), spectral features (Hawley et al. 2002; Bochanski et al. 2007b) and luminosity and mass functions (Bochanski et al. 2010) of these ubiquitous stars have all been extensively examined with SDSS data. Other studies have used these stars as tracers of local Galactic structure (Jurić et al. 2008; Bochanski et al. 2010) and kinematics (Bochanski et al. 2007a; West et al. 2008; Ivezić et al. 2008; Fuchs et al. 2009; Schmidt et al. 2010; Bond et al. 2009). Studies on the temporal behavior of M dwarfs have included examinations of chromospheric variability (Kruse et al. 2010), flare rates (Kowalski et al. 2009; Hilton et al. 2010) and periodicity (Bhatti et al. 2010; Blake et al. 2008).

Eclipsing M dwarf systems are particularly valuable because they provide the opportunity to measure the masses and radii of the stars through spectroscopic radial–velocity followup. Current M dwarf stellar evolution models do not match physical properties measured from known eclipsing systems, with the models system-

---

[1] Astronomy Department, University of Washington, Seattle, WA 98195
[2] Astronomy and Astrophysics Department, Pennsylvania State University, 525 Davey Laboratory, University Park, PA 16802
[3] Boston University, Department of Astronomy, 725 Commonwealth Ave, Boston, MA 02215

atically underpredicting the radius of these stars at a given mass (e.g. Baraffe et al. 1998; Ribas 2006). Several explanations have been proposed to explain this discrepancy, typically relying on enhanced magnetic activity due to coupling of the stellar rotation with the system orbital period. Elevated activity may also arise due to the lack of disk locking early in the angular momentum evolution of close pairs, which allows the individual stars to rotate much faster (and generate stronger magnetic fields) than individual low–mass dwarfs (Artymowicz & Lubow 1994). Elevated magnetic activity should lead to increased coverage by star spots in the stellar photosphere; polar spot systems covering 35% of the star with a moderate contrast ratio have been shown to both be plausible and to cause systematic overestimates of the true stellar radius in eclipsing binary studies (Morales et al. 2010). The enhanced magnetic field may also suppress convective turbulence (and thus heat transfer) to the surface of the star, requiring the stellar radius to increase to maintain its luminosity (López-Morales 2007; Chabrier et al. 2007). If caused by orbital coupling, these effects should become less pronounced for stars with long orbital periods and thus large semi–major axes (unless they are already rapidly rotating due to their youth). Therefore, eclipsing systems with a range of orbital periods are needed to quantify these effects. To date, most known eclipsing M dwarf systems have been discovered with short orbital periods, < 10 days, where spin–up due to orbital coupling is expected to be strong (Mazeh 2010). An additional transition in the mass–radius relationship might be expected at the boundary between partially and fully convective stars (Mullan & MacDonald 2001; Baraffe et al. 1998), requiring the discovery of faint stars across this transition (expected near spectral types M3–M4) to characterize it empirically. With these goals in mind we have undertaken a data mining study on a photometric database of SDSS Stripe 82 to identify low–mass eclipsing binary systems.

2. THE STRIPE 82 DATABASE

While the majority of SDSS imaging resulted in a single epoch of data, imaging of SDSS Stripe 82 was undertaken during commissioning (starting in 1998) and repeated intermittently throughout the survey. Stripe 82 covers 300 $\deg^2$ of the SDSS footprint, with $-60^\circ < \alpha < +60^\circ$ (20 h to 4 h in right ascension, RA) and $-1.267^\circ < \delta < +1.267^\circ$ in declination (Dec). Stripe 82 was imaged every clear night for 3 months of the year as part of the SDSS-II Supernova Survey from 2005–2007 (Frieman et al. 2008). In contrast to the main survey, supernova observations were taken in non–photometric conditions, making recalibration of these data a necessity (Ivezić et al. 2007). The primary science driver was the discovery and characterization of Type Ia supernovae to study the equation of state of the dark energy revealed by precursor supernova surveys (Riess et al. 1998; Perlmutter et al. 1999). As described in Sako et al. (2008), great care was taken to reject non supernova–like phenomena during the real–time portion of the survey. While this led to a very high (90%) photometric Ia typing and targeting efficiency, it also meant that the majority of the transient phenomena have not yet been studied in detail. Targeted studies of these foreground events have shown that the Stripe 82 data are rich with new and interesting phenomenology. Particular cases include discoveries of a new AM Canum Venaticorum system (Anderson et al. 2008), new ultracool and halo white dwarf systems (Vidrih et al. 2007), and a new class of inner Oort Cloud objects (Kaib et al. 2009). Studies of subsets of the Stripe 82 data have been undertaken by Sesar et al. (2007), Bramich et al. (2008), Watkins et al. (2009), Bhatti et al. (2010), and Sesar et al. (2010).

We have followed the prescription of Ivezić et al. (2007) in recalibrating the publicly available Stripe 82 dataset. The resulting MySQL database currently holds observations from 600,727 $9' \times 13'$ fields acquired during 251 observing runs. The earliest run was taken as part of commissioning science on 1998/09/19, while the latest run was acquired as part of the Supernova Survey on 2007/10/19. The database includes 204,527,387 single–epoch 5–band source measurements, with corresponding PSF magnitudes, celestial coordinates, and effective times of observation. These individual observations are clustered using the `OPTICS` (Ankerst et al. 1999) algorithm into [7,913,421; 4,793,517; 1,418,977] objects with temporal lightcurves containing at least [3; 10; 50] observations. Higher order statistics are also available for each lightcurve (mean, median, standard deviation, skew, kurtosis, χ^2 per degree of freedom).

The measured zeropoints of Stripe 82 images have an RMS of $0.009, 0.004, 0.003, 0.003, 0.004$ magnitudes in the u, g, r, i, z bands, respectively, about the SDSS standard photometric system. This reflects the quality of the absolute calibration of the data. The photometric scatter about the median for bright stars (between 15^{th} and 17^{th} magnitude in a given passband), which reflects the systematics inherent in the photometry, is $0.025, 0.024, 0.014, 0.016, 0.020$ magnitudes for the u, g, r, i, z bands, respectively. This relative calibration is slightly worse than that derived from the subset of the data analyzed in Sesar et al. (2007). However, the larger number of photometric measurement used here (205 million vs. 34 million for Sesar et al. (2007)) were acquired over a larger range of observing conditions, many of them during the SDSS-II Supernova Survey. The ability to maintain $\sim 2\%$ relative calibration with such a large ensemble of data enables new avenues of precision astronomy.

2.1. *Period Estimation*

We searched for periodicity in all Stripe 82 lightcurves having more than 10 epochs using the 1024–node "Athena" computing cluster at the University of Washington. We used the variable–span `Supersmoother`[4] algorithm of Riemann (1994) for period estimation (see also Oh et al. 2004). For a given period estimate, `Supersmoother` implements running linear smooths of the data at multiple span lengths, using a localized cross–validation to determine the optimal span. Period estimates are then ranked by the sum of absolute residuals about each optimally smoothed model, with the "best" period yielding the smallest residuals. `Supersmoother` is able to uncover a variety of lightcurve shapes because it makes no explicit assumptions about the underlying shape of the curve, except that when folded it be smooth and continuous. Since the algorithm does not return an explicit uncertainty (or false alarm probability) on the period, we used the fact that we have multiple constraints on the true period from the g, r, and i–band lightcurves (which typically have the smallest photometric errors). We addressed each passband's data separately, applying `Supersmoother` to the entire calibrated lightcurve. The derived periods in the g, r, and i data are referred to as P_g, P_r, and P_i. We only considered the *best* period, as determined by the sum–of–absolute–residuals, for each of the three passbands.

---

[4] Available upon request

We used concordance between the periods returned in each of the 3 passbands to make an assessment as to the true period (if any) in the data. We required one of the following three matching criteria be met before we considered the object a periodic candidate:

- The standard deviation of P_g, P_r, and P_i is less than 10^{-5} times their average value;
- A similar test as the one above but applied to each period modulo the minimum of the three periods (to account for period aliasing);
- The standard deviation of two of the three values of P_g, P_r, and P_i is less than 10^{-4} times their average value. This allowed us to diagnose cases where `Supersmoother` returned an aberrant period for one of the lightcurves, or when the "correct" period was reported as the second or third best for one of the lightcurves.

As an additional step, we rejected those lightcurves where the matched period was longer than 365 days, or was within 0.01 days of the single–day sampling alias. These criteria resulted in a manageable number of periodic candidates (10^3) that could be investigated through visual inspection.

2.2. *Color Selection of our Catalog*

We have chosen to focus here on the extraction of periodic variability for low–mass stellar systems. The photometric calibration of our database allows us to accurately select low–mass systems based upon their mean colors[5]. We outline the two sets of color selection criteria below.

2.2.1. *M dwarfs*

We selected likely M dwarf systems using a mean–color selection criteria of $r - i > 0.5$ and $i - z > 0.3$ (Bochanski et al. 2007a). This initial cut returned 3,301,051 objects. Using the period concordance tests described in Section 2.1, we selected 1,387 candidate periodic systems. Finally, a visual inspection of these lightcurves (Section 2.3) resulted in 203 candidate M dwarf systems. In addition, we further identified 42 of these systems as likely M dwarf / white–dwarf pairs using the color–selection criteria ($u - g < 1.8$) of West et al. (2004).

2.2.2. *White Dwarfs*

We made a separate, independent set of cuts to identify systems with white dwarf components : $u - g < 0.7$ and $g - r < 0.5$ (Ivezić et al. 2007) . Objects passing both these cuts and the cuts of Section 2.2.1 are likely to be M dwarf/white–dwarf pairs (e.g. Smolčić et al. 2004). We found 421,682 objects that passed this basic color test, 172 that passed our period selection criteria, and only seven that passed visual inspection. Four of these are unique from the M dwarf sample.

2.3. *Visual Inspection*

For each system that passed our period criteria, we folded the lightcurve at that period and visually inspected the phased data. This helped to reject spurious systems, as well as to classify the nature of the variability. We used the continuity of the folded lightcurves, with respect to the photometric error bars, to ascertain if the system is periodic.

During this process we noted that some returned periods were obvious aliases of the true period; for example an eclipsing system with two different depth minima folded at half its period will have a bimodal lightcurve in eclipse. We therefore report here the periods that resulted in two maxima and minima in the folded lightcurves. We thus expect that our periods represent the *maximum* system period.

3. CATALOG OF PERIODIC VARIABLES

Table 1 provides a summary of the 207 systems found in this process[6]. Each object is identified using a unique designation derived from its mean right ascension and declination (J2000). We also derive the error–weighted mean r–band magnitude and the mean colors of the system using all measurements. We have de–reddened each observation using the extinction maps of Schlegel et al. (1998), since the majority of systems are presumed to lie beyond the dust layer (Marshall et al. 2006).

We offer a qualitative assessment of each phased lightcurve in Table 1. Lightcurves with grade `A` (21 out of 207) are the best candidates, with complete and even phase coverage, and a smooth folded lightcurve shape. Lightcurves with grade `B` (115 / 207) are typical candidates, with some gaps in the phase coverage leading to some uncertainty in the overall lightcurve shape, but with enough coverage that the periods are likely correct. Lightcurves with grade `C` (71 / 207) are lower S/N candidates, with noisy lightcurves and larger–than–average gaps in phase coverage. These will require additional photometric follow–up for period confirmation; however they are included here due to the suggestive shape of the phased lightcurves.

3.1. *Comparison with Bhatti et al. (2010)*

Recently Bhatti et al. (2010) published a catalog of the 0 hour < RA < 4 hour portion of Stripe 82, with particular attention paid to periodic variability. They find 32 eclipsing or ellipsoidal binaries in this region of sky (Table 2; Bhatti et al. 2010), only 11 of which pass our

---

[5] For completeness we note that we do not apply an extinction correction before the color selection defined below. Therefore some de–reddened colors listed in Table 1 are slightly outside the color selection criteria defined in Section 2.2.1 and Section 2.2.2.

[6] Data are available at http://www.astro.washington.edu/users/becker/dataRelease/stripe82Periodic/

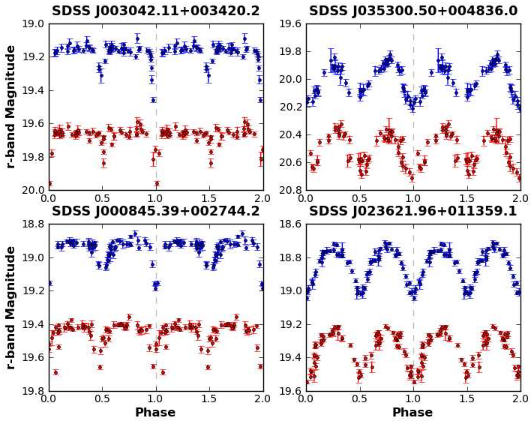

Figure 1. r–band lightcurves for the four objects where our periods do not agree with the Bhatti et al. (2010) periods. In each panel, the *top* lightcurve shows the data folded at the periods derived in this analysis. The *bottom* lightcurve shows the data folded at the Bhatti et al. (2010) periods, with an 0.5 magnitude offset added for clarity. We show the folded lightcurves for two oscillations. For all four objects, both sets of folded lightcurves are generally coherent; however the periods derived in this analysis appear to result in lightcurves showing fewer outliers. This is verified by undertaking a Fourier analysis of the folded lightcurves; in all cases the χ^2 for lightcurves folded at the periods derived here are smaller, suggesting our periods are the correct ones.

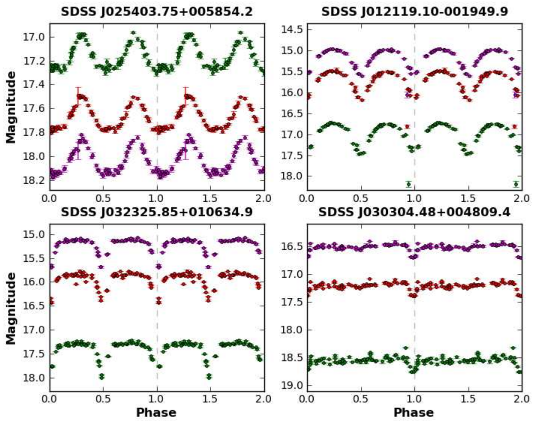

Figure 2. g, r, and i–band lightcurves for four objects found in our analysis but not in the Bhatti et al. (2010) analysis. Each panel shows the three passbands of data folded at each object's period, listed in Table 1. Top–to–bottom the lightcurves appear in the order i, r, g, except for the blue system SDSS J025403.75+005854.2 in which the order of the lightcurves appears reversed. For SDSS J030304.48+004809.4 the secondary minimum near phase 0.5 is barely detectable, but is most apparent in the i and z–band (not shown) data. We show two oscillations of each lightcurve. The top 2 lightcurves were manually graded as `A`–quality lightcurves, SDSS J032325.85+010634.9 as `B`–quality, and SDSS J030304.48+004809.4 as `C`–quality (Section 3).

color–selection criteria. The remaining 21 are not included in our analysis due to their average colors. However, to compare with the Bhatti et al. (2010) results, we manually performed our `Supersmoother` analysis on these 21 objects. Table 3 compares our period estimates for both classes of objects – those that pass our color cuts, and those that do not. We list our derived periods along with ratios of the periods found in the two studies (recall that periods here have been aliased to result in lightcurves with two maxima/minima, and are expected to represent the maximum likely period for the system).

For four of the objects listed in Table 3, our analysis found a period that was not an exact match to, or an alias of, the Bhatti et al. (2010) period. Figure 1 shows the folded r–band lightcurves of these four objects : SDSS J003042.11+003420.2, SDSS J035300.50+004836.0, SDSS J000845.39+002744.2, and SDSS J023621.96+011359.1. For each panel, the lightcurve resulting from the periods derived in this analysis is shown on the top, and the lightcurve folded at the Bhatti et al. (2010) period is shown below with a +0.5 magnitude offset added for clarity. Both datasets appear to show the overall coherence expected of a periodic lightcurve folded at its correct period. However, the top set of lightcurves (resulting from our periods) show fewer outliers. We quantify this by undertaking a Fourier decomposition of the lightcurves using Equation 1 (defined in Section 4.2) and comparing the χ^2 between the model fits to the datasets folded at the two periods. This comparison yields $\chi^2_{\rm Bhatti} - \chi^2_{\rm Becker} = [7; 119; 355; 217]$ for r–band Fourier decompositions of SDSS [J003042.11+003420.2; J035300.50+004836.0; J000845.39+002744.2; J023621.96+011359.1], respectively. This verifies that our periods are ones best supported by our data.

For five of the objects, our analysis failed to find consistent periods in the g, r, and i–band data. For three of these, the Bhatti et al. (2010) period is found as the second–best period. For the other two, we do not find the Bhatti et al. (2010) period in the top 3 periods, for any passband. This includes the eclipsing binary from Becker et al. (2008), which was originally discovered in data from the Two Micron All Sky Survey (Skrutskie et al. 2006) and also found in the Stripe 82 catalog of Bhatti et al. (2010). Our corresponding lightcurve only shows one data point per eclipse minimum, and thus we were unable to derive an orbital period. This is evidence that the Bhatti et al. (2010) data and ours differ both in calibration and in content.

Finally, we examine those objects not contained in the Bhatti et al. (2010) sample. With our color cuts, we find 60 periodically variable objects between 0 h < RA < 4 h. Of these, only eight are found by Bhatti et al. (2010). We have checked that the 52 missed candidates do not correspond to stars identified by Bhatti et al. (2010) as RR Lyrae or δ Scuti, and have verified from our lightcurves that the objects appear truly periodic. We display the folded g, r, and i–band data for four of these objects in Figure 2. Bhatti et al. (2010) estimate $\sim$ 55% efficiency at recovering known input periods. Since we find a factor of 7–8 times more periodic variables in the same sample that they analyzed, its likely that the discrepancy arises due to differences in internal photometric calibration procedures, along with differences in our respective period–finding algorithms. We estimate our own period recovery efficiencies below.

3.2. *Efficiency of Period Recovery*

To assess the uncertainties on Supersmoother's best–fit periods given the particular properties of Stripe 82 data, including sampling rate and photometric error bars, we undertook a Monte Carlo simulation to determine our pe-

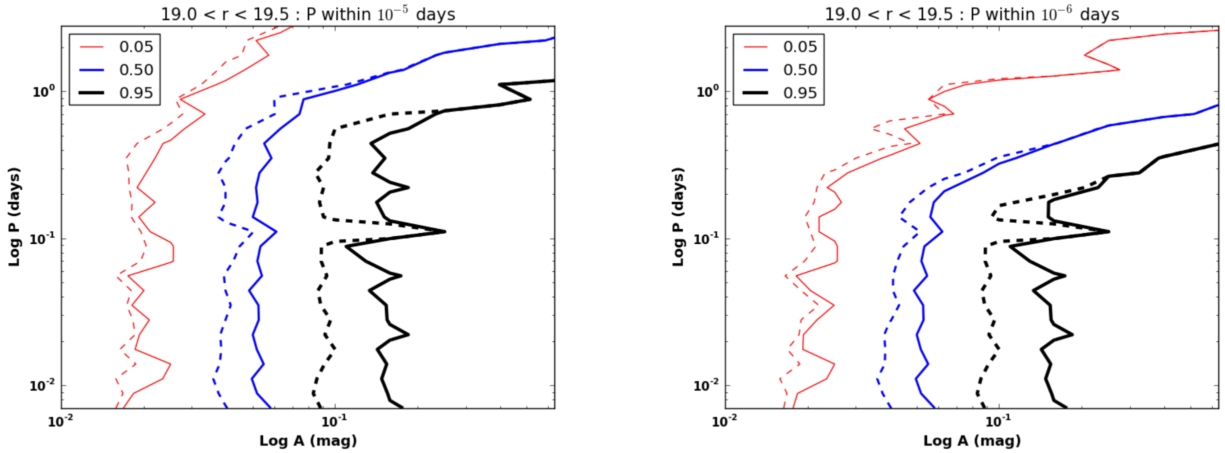

Figure 3. Contours showing the efficiency of period recovery as a function of lightcurve period P and amplitude A, for sinusoidal variables in the brightness range $19.0 < r < 19.5$. The *left* panel shows the recovery fraction under the matching criterion $|P_{fit} - P_{input}| < 10^{-5}$. The *right* panel shows these results when the matching criteria are tightened to $|P_{fit} - P_{input}| < 10^{-6}$. The recovery is effectively the same except for at longer periods, where the objects have gone through fewer oscillations during the Stripe 82 observing window. The solid contours show the 5%, 50%, and 95% recovery efficiency when only the best–fit period is considered. The dashed contours reflect a loosening of the matching criteria to also define as matches cases where P_{fit} is a 2–times alias of P_{input}. This is most important for moderate amplitude lightcurves, and at the shorter periods.

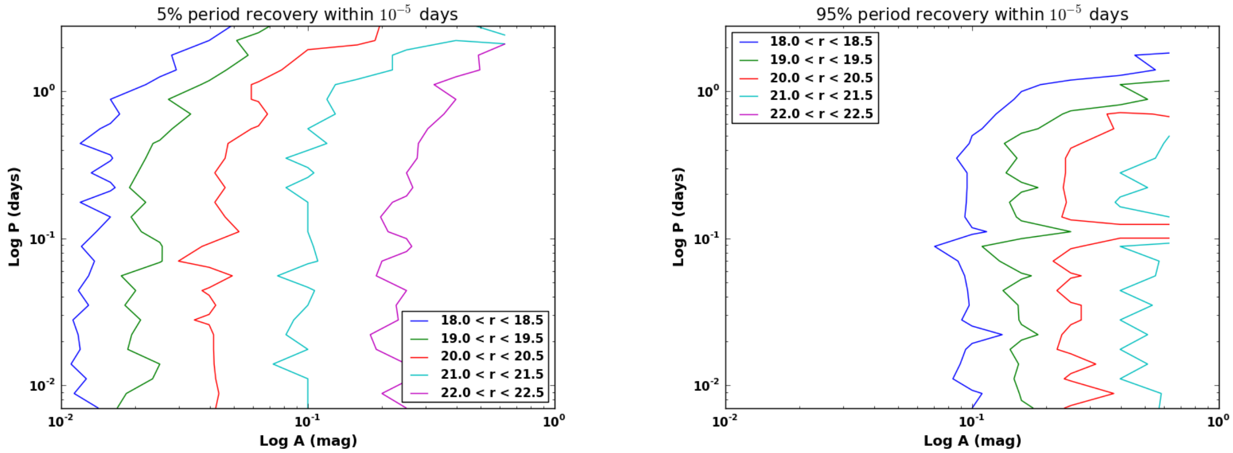

Figure 4. Contours showing the efficiency of 5% (*left*) and 95% (*right*) period recovery as a function of period, amplitude, and source brightness, using the matching criterion of $|P_{fit} - P_{input}| < 10^{-5}$. If we include fitted periods that are double the true period, which an observer is likely to recognize as an alias upon lightcurve folding, we are able to extend 5% recovery ~ 0.02 mag smaller in amplitude, and 95% recovery $\sim 0.05 - 0.1$ mag smaller in amplitude, at a given source brightness.

riod recovery efficiency. We first defined brightness bins between $r = 18$ and $r = 22$ in steps of 0.5 magnitudes, to assess the impact of source brightness and photometric error on period recovery. Within each magnitude bin, we randomly selected 100 stars from the database whose intrinsic lightcurves have a reduced $\chi^2 < 1$, where this random selection allows us to define an average lightcurve sampling across the Stripe 82 region.

We next defined a range of shapes, periods, and amplitudes to study. Given the breadth of lightcurve shapes allowed in eclipsing systems, we decided to limit our analysis to sinusoidal lightcurves for its computational simplicity, meaning our analysis is likely optimistic for the detached sample, especially those lightcurves spending small fractions of their duty cycle in eclipse. We investigated sinusoidal lightcurves having a range of periods P between $-2.15 < \log(P) < 0.445$ (0.007 to 2.786) days in steps of $\Delta \log(P) = 0.1$. We also investigated a range of amplitudes A for the lightcurves with $-2 < \log(A) < 0.2$ (0.01 to 0.63) magnitudes, in steps of $\Delta \log(A) = 0.2$. For each object, we modified the r–band lightcurve with the variability imprint defined by each combination of period and amplitude, defined as $\Delta\, r = A\ \sin(2\pi\phi + \varphi)$. Here ϕ is derived from the epoch of observation T as $\phi = T/P - T//P$, where the // operation generates the integer portion of T/P. The variable φ was generated randomly and represents a shifting of the zero point of the lightcurve.

We ran each modified lightcurve through `Supersmoother` and compared the recovered period with the known input period. We show the results for the bright end of this sample ($19 < r < 19.5$) in Figure 3. For each combination of P and A, this figure shows the fraction of the 100 input stars whose period was recovered to within 10^{-5} days (*left* panel) and 10^{-6} days (*right* panel). The solid contours at 5%, 50%, and 95% recovery are for comparing the best–fit period to the true period, while the dashed contours includes the additional fraction of fitted periods that were 2–times aliases of the true period. In the latter case, an observer is likely to recognize upon period folding that the fitted period is an alias, and classify the lightcurve as periodic. The surface shows nearly 100% period recovery at high amplitude ($A > 0.2$ mag) below 0.5 days. At periods longer than 0.2 days this efficiency falls rapidly when the matching criteria are tightened from 10^{-5} days to 10^{-6} days. This is understandable as at longer periods the objects go through fewer oscillations during a given temporal window. By including aliased–by–2 periods, we can extend this recovery down to $A > 0.09$ magnitudes. We are not likely to recover any periodic lightcurves with amplitudes smaller than 0.02 mag at all periods.

We examine how this matching degrades as the source brightness is decreased in Figure 4. In the *left* panel we plot the 5% recovery contours for 5 of the magnitude bins, and in the *right* panel the 95% recovery contours, for exact period matches. On average, if we also consider aliased–by–two periods we can extend the 5% recovery level 0.02 magnitudes smaller in lightcurve amplitude, and the 95% recovery level $0.05-0.1$ magnitudes smaller in amplitude, at a given source brightness. The overall efficiency profiles suggest that the dearth of objects in our catalog with periods longer than ~ 1 day may plausibly be explained by our low period recovery efficiency at these long periods, at all source brightnesses. Similarly the lack of systems fainter than $r = 20.5$ may be explained by a precipitous drop in efficiency at all but the largest amplitudes. Our high efficiency at bright magnitudes cannot alone explain our larger yield from the Stripe 82 data compared to the Bhatti et al. (2010) analysis.

4. CLASSIFICATION

In Table 2 we provide rough classifications of all systems, in order to help enable photometric or spectroscopic follow–up observations.

4.1. *Spectral Type*

We found SDSS DR7 (Abazajian et al. 2009) spectra for 29 of our objects, including 27 whose spectra indicate they contain at least one M dwarf member. All but one of the M dwarf systems (26 of the 27; 96%) show signs of chromospheric magnetic activity (as traced by Hα emission). This is considerably higher than the magnetic activity rate seen in the field (24%, West et al. 2004) for a similar distribution of spectral types. This high rate of magnetic activity confirms previous results from close binaries, as compared to their field counterparts (Silvestri et al. 2006).

We next used the mean system colors, as well as the spectra when available, to estimate spectral types. The results are given in Table 2. The *Color Class* is an estimate of the spectral type of the system using broad–band colors and the color–spectral type relations of Kowalski et al. (2009). Systems with $u - g < 1.8$ are labeled with a "+WD", indicating a white dwarf companion (West et al. 2004). The objects with spectra were typed using the `Hammer` software described in Covey et al. (2007), resulting in our *Spectral Class* estimation. The *Color* and *Spectral* classes typically agree to within 1 subtype.

4.2. *Binary Type*

We evaluate the lightcurves under the assumption that each is an eclipsing binary system with two minima in its lightcurve. The standard classification scheme for eclipsing binary systems uses the following categories:

- EW : W UMa–type (classical contact) binaries where both stars are surrounded by a common convective envelope (Lucy 1968). Primary and secondary eclipse depths are typically similar in depth due to the constant effective temperature of the envelope.
- EB : EW–type binaries with different eclipse depths. The archetype is β Lyrae. However this particular lightcurve shape may result from a variety of physical configurations, including semi–detached binaries or thermal relaxation oscillations in EW systems (Flannery 1976).
- EA : Detached binary stars, where both objects are contained completely within their respective Roche lobes.

Pojmanski (2002) has defined an empirical means of separating these systems into analogous classes describing the *geometry* of the system, through the use of a Fourier decomposition of the folded lightcurve. His classes are EC (contact, analogous to EW systems), ESD (semi–detached, analogous to EB), and ED (detached, analogous to EA). We performed a decomposition of the g, r, and i–band lightcurves of the form

$$m(\phi) = A_0 - \sum_{i=1}^{4} A_i \cos(2\pi i\phi + \varphi) + B_i \sin(2\pi i\phi + \varphi) \tag{1}$$

Here A_0 represents the mean brightness of the system, ϕ corresponds to the phase, and φ is a nuisance parameter defined such that the model has minimum brightness at $\varphi = 0$. We use the Pojmanski (2002) polygons defining the EC, ESD, and ED regions in the two–dimensional space of Fourier coefficients A_2 and A_4, as displayed in Figure 5. Additionally, Rucinski (1997) provides a discriminant between contact and detached systems through the relationship $A_4 = A_2 * (0.125 - A_2)$, shown as the *dashed* line in Figure 5. Objects lying above this line are more likely to be in contact, while objects lying below this are more likely to be detached. We use this boundary to provide asterisked classifications for contact (EC^*) and detached (ED^*) systems laying outside the polygon boundaries of Pojmanski (2002). We note that the Pojmanski (2002) regions overlap, and thus our objects may receive more than one classification per passband. Classifications per passband for all objects are given in Table 2.

5. RESULTS

We emphasize that the strength of this catalog is not solely in the *number* of eclipsing binary systems found,

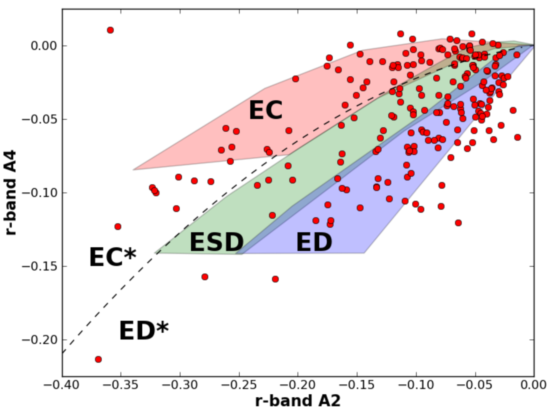

Figure 5. r–band Fourier components A_2 and A_4 for our periodic sample. Typical uncertainties on A_2 and A_4 in the Fourier fits are $\sim 0.02 - 0.03$ magnitudes, as estimated by the non–linear minimizer `MINUIT`. The three patches correspond to the contact (EC), semi–detached (ESD), and detached (ED) boundaries as defined by Pojmanski (2002). For those systems that lie outside these regions, classification occurs using the *dashed* line of demarcation between contact (EC*) and detached (ED*) of Rucinski (1997).

but that through color and spectral–typing they have been verified to contain low–mass stellar components. We examine in detail subsets of our data below, for those systems whose classifications agree in the g, r, and i–band data.

5.1. *ED M dwarf Systems*

Table 2 contains 59 systems whose colors are consistent with being M dwarfs, inconsistent with having a white dwarf companion, and whose lightcurves shapes in g, r, and i are consistent with the detached classification (ED or $ED*$) of Pojmanski (2002) and Rucinski (1997). This increases by a factor of several the number of published detached candidate systems (however see also Shaw & López-Morales 2007). Such systems are needed to examine the mass–radius relationships of low–mass stars (Section 1).

Only 11 stars in this subsample have orbital periods greater than 1 day, with the maximum period being 2.76 days for J003841.29+010756.0. There are only 2 data points in eclipse for this system, and we have classified this as having a C–quality lightcurve. There is however coherent out–of–eclipse variability that leads us to include this system in our sample. Since all our M dwarf ED systems have short orbital periods, they are likely being spun–up through orbital coupling, and their radii influenced by the enhanced magnetic field. This sample also contains 7 systems classified as M4–M5, which are expected to be fully convective (Burrows et al. 1993; Mullan & MacDonald 2001). Their mass–radius relationship is expected to be less affected by convection–related orbital coupling effects, but may still be affected by enhanced spot coverage (e.g. Morales et al. 2010).

5.2. *EC M dwarf Systems*

Twenty–eight of the M dwarf lightcurves have shapes that suggest they are in contact configurations (EC or $EC*$, as defined in Section 4.2). This is a surprising outcome given the lack of such systems in the literature. The shortest period eclipsing M dwarf system verified so far, BW3 V38 (Maceroni & Rucinski 1997) with a period of 0.1984 days, is shown to be highly distorted but *not* in contact. Thus we caution that while our lightcurve shapes may yield a $EC/EC*$ classification, our systems may not be physically in contact, and will require further study for any definitive statements. However, the short periods of these systems are consistent with their sinusoidal lightcurves, both of which indicate a compact binary configuration.

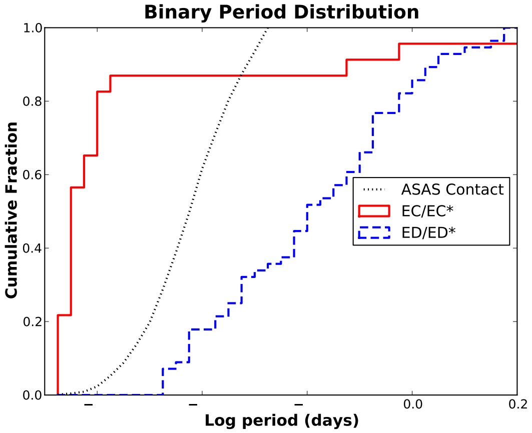

Figure 6. Cumulative distribution of orbital periods derived for the subset of our systems that have the colors of M dwarfs, no evidence for white dwarfs in either their $u - g$ colors or in spectra (if available), and whose lightcurve shapes in the g, r, and i passbands are in concordance about being in contact (*red, solid* line) or detached (*blue, dashed* line) configurations, using the classification schemes of Pojmanski (2002) and Rucinski (1997). Our contact systems show a significant pile–up between $-0.65 < \log(P) < -0.58$ (0.22 and 0.26 days). We contrast this with the distribution of contact binary periods derived by Rucinski (2007) based on All Sky Automated Survey (ASAS) data (*black, dashed* line). These represent earlier–type stars, and are typically found at longer periods than our M dwarf–classified sample.

Our period distribution for $EC/EC*$ systems demonstrates a steep cutoff near 0.22 days (log P = -0.65), a feature seen in period distributions of earlier–type contact systems (e.g. Paczyński et al. 2006). There is however one notable difference: the vast majority of our binaries (24 / 28) are accumulated near this period cutoff, with an RMS of 0.02 days. These 24 candidates all have A or B–graded lightcurves, as described in Section 3. In addition, 22 of them are brighter than $r = 19$, where our efficiency analysis in Section 3.2 shows that the median mis–fit in period at amplitudes larger than $A = 0.016$ mag (a condition matched by all objects) is less than 10^{-6} days, meaning the presence of this peak is established at high significance.

Thus, our sample of periods has a far smaller variance than is seen in the AFGK spectral–type contact binary population (Rucinski 2006), and densely populates the short period end of the distribution. We display in Figure 6 the distribution of periods for our contact (*red, solid* line) and detached systems (*blue, dashed* line). It is clear that the majority of contact systems are found at shorter periods than the detached sample. We also show the contact binary period distribution derived by Rucinski (2007) using all–sky bright–star data (ASAS contact binary sample; *black, dashed* line), which spans the approximate spectral types from A–K. Compared to the earlier–type, bright–star periods, our systems are found at much shorter periods on average.

Stepien (2006) has proposed a lower limit on the total mass of current–day contact systems of $\sim 1M_\odot$, based upon the 0.22–day cutoff seen in previous survey data. Contact systems with less total mass than this are not expected to be seen, since their evolutionary timescales to Roche lobe overflow are longer than the age of the Universe. Our observed accumulation of M dwarf periods near this cutoff supports evolutionary processes where angular momentum loss becomes less efficient at shorter orbital periods, which then suppresses the evolution to even shorter period systems. Interestingly, two $EC/EC*$–classified systems have periods less than 0.2 days, SDSS J200011.19+003806.5 (0.1455201 days) and SDSS J001641.03-000925.2 (0.1985615 days). Of these two, SDSS J001641.03-000925.2 has the higher quality lightcurve and a detailed study of this system is forthcoming (Davenport et al., in preparation).

We have matched each of these 24 objects with the nearest simulated lightcurve from our efficiency analysis in magnitude, period, and amplitude and find that most of the objects were expected to be detected at high ($\geq$ 90%) efficiency, with the exceptions of SDSS J035856.16+004010.2 (66%), and SDSS J202617.44-003738.6, J202247.66-002902.4, and J231823.93-004415.2 (77%). Using the efficiency per object to weight the sample, we find 0.087 EC–type M–dwarf binaries per square degree over the nominal magnitude range $14 < r < 21.5$.

5.3. *ED M dwarf/White Dwarf Systems*

Forty–two systems have blue colors (in $u - g$) consistent with having a white dwarf component, and red colors (in $r - i$ and $i - z$) consistent with having an M-dwarf component. Eleven of these are classified as being detached type ED/ED^*. Most of these ED–classified systems have longer periods ($0.4 - 0.9$ days) than expected for current cataclysmic variable (CV) systems (e.g. Figure 9 of Howell et al. 2001). The consistency between the lightcurve shapes (suggesting detached systems) and the periods (suggesting pre–CV and thus pre–contact configurations) lends support to our interpretation of the systems.

Wide (detached) CV–progenitor systems should currently have low mass accretion rates, with heating (if any) of the accretor occurring through light particle winds as opposed to streaming accretion (e.g. Szkody et al. 2003). Multi–wavelength follow–up of these systems should be able to resolve the nature of any active accretion (Szkody et al. 2008).

5.4. *EC M dwarf/White Dwarf Systems*

Ten systems have colors and shapes consistent with being a contact (type EC/EC^*) M dwarf / white dwarf binary. These appear to be eclipsing CV systems (e.g. Howell et al. 1997, and references therein). All but two of the 10 EC systems (J233538.33-002927.3 and J234309.23-005717.1) have periods less than 0.26 days, well within the period range expected for early CV systems (Kolb 1993). The shortest of these, J013851.54-001621.6 (Becker et al., in preparation), has a period of 0.072765 days, below the "period gap" expected from CV evolution models (Howell et al. 2001) and where the majority population of the current CVs are thought to reside (Howell et al. 1997). The EC lightcurves are too sparsely sampled to allow us to constrain the properties of any accretion–related effects such as hot spots. However, the average lightcurve color–variations in $u - g$ for these EC–classified systems ($< \Delta(u - g) >= 0.09$ mags) is larger than in the EC systems that have no indications of white dwarf companions ($< \Delta(u - g) >= 0.03$ mags).

5.5. *Systems With No Evidence of M dwarfs*

Four of the systems pass our white–dwarf selection criteria, but do not pass our M dwarf selection criteria. Of the four, SDSS J212531.92-010745.8 has previously been studied by Nagel et al. (2006) who concluded that it has a pre–degenerate hot (PG 1159–type GW Vir) primary and faint M dwarf secondary being irradiated by the primary. Their derived orbital period is exactly 0.5 times ours, indicating that our requirement of folded lightcurve shapes with two minima has led to an alias in our period estimate. We note that the lightcurve of SDSS J025403.75+005854.2 is extremely similar, and is a promising candidate for another PG 1159–type system.

6. DISCUSSION AND CONCLUSIONS

We have described a data–mining effort to extract periodic stellar variability from the SDSS Stripe 82 dataset. The power of this catalog lies in multi–color, time–domain photometry that enables characterization of the components and systems, as well as precise period estimates. To emphasize the immediate utility of these data, we have focused here on periodic variability of low–mass stars. We detect 161 eclipsing systems whose light is dominated by a red, M dwarf component, 42 systems composed of an M dwarf white dwarf pair, and four systems whose light is dominated by a white dwarf member with no evidence of an M dwarf companion. We have additionally used the shape of the lightcurves to classify the geometrical nature of the binary (contact, semi–detached, detached) using the classification schemes of Pojmanski (2002) and Rucinski (1997).

Overall, the systems at the shorter periods have folded lightcurves that are classified as "contact", while the longer–period systems tend to have lightcurves classified as "detached". We emphasize that the processes of determining the period, and of determining the geometric system configuration through Fourier decomposition of the folded lightcurve, are entirely independent stages in the analysis. While the classification of any given system may be uncertain, requiring additional photometric and spectroscopic follow–up, our independent classification processes generally give good agreement.

We have run an efficiency analysis to estimate our recovery of variable star periods over a range of magnitudes, periods, and amplitudes. This process was only undertaken for sinusoidally–shaped lightcurves, meaning it is not strictly appropriate for the detached sample. Even for this subset of shapes, the required processing time was substantial, and required a compute cluster to undertake in a reasonable amount of time. We generated 243000 fake lightcurve, each of which took of order 10 minutes to process through `Supersmoother` searching all possible periods longer than 0.007 days. This amounts to 4.6 CPU–years of processing time for this trivial shape set. To additionally explore the recovery efficiencies for the detached sample, with a range of eclipse frequencies, depths, and durations, would amount to an enormous computational undertaking.

The initial aim of our investigation was to provide additional systems to study the mass–radius relationship of M dwarf systems in binaries. However, the majority of our detached systems are in the "typical" short–period configuration of published eclipsing M dwarf systems, and are thus not likely to resolve the origin of the mass–radius discrepancy, since this requires a longer lever–arm in orbital period than our catalog provides. The optimal set of data to address the source of the mass–radius discrepancy should include both short period and long–period systems, to study the degree to which orbital spin–up affects convection and/or star spots and thus the stellar radius. The study of mass–radius relations at the transition from partially to fully convective stars (around M3–M4) may help to shed light on the role convection plays in this process. Our catalog provides 7 systems classified as M4–M5, which should also be useful in this regard.

The most unexpected component of the catalog is the number of classical "contact" (EW–type) lightcurves. M dwarf systems physically in contact are not expected since the predicted time to Roche lobe overflow is longer than the Hubble time (Stepien 2006). The period distribution of these systems does suggest that they are following the same dynamical pathway as earlier spectral type contact systems, having the steep cutoff at 0.22 days that is seen in other surveys. However, the variance of the period distribution in low–mass binaries is far smaller than seen for earlier spectral type stars. This "pile up" at 0.22 days suggests that period evolution is becoming far less efficient as the orbital period decreases. Study of these extreme, highly coupled, systems will help constrain the degree to which orbital spin–up affects the stellar radius at the shortest periods. If such effects are larger in systems with shorter periods, it will impact stellar evolution and mass–loss models that predict the timescale to Roche lobe overflow. Using our efficiency analysis, we estimate a density of 0.087 such systems per square degree, over the brightness range $14 < r < 21.5$.

Our M dwarf / white dwarf sample includes both close and wide eclipsing CV–type systems, which should probe a range of mass transfer rates and the resulting heating of the white dwarf component. We also detect one known PG 1159–type system, with a second (new) system showing similar–type variability.

Substantial amounts of observing follow–up, both photometric (to more tightly constrain the periods and shape of the lightcurves) and spectroscopic (to constrain radial velocities and to more thoroughly understand the stellar atmospheres), are needed to fully realize the potential of this catalog. We approximate the total amount of spectroscopic follow–up time needed to map radial velocity (RV) curves for all 207 systems, using the Magellan Echellette (MagE) spectrograph as our benchmark instrument. Integrating for 1500 seconds with MagE ($R = 5000$) yields a signal-to–noise of approximately 50 at $r = 19$, sufficient for $\sim$ 5 km/s uncertainties per radial velocity point. If we require 5 RV measurements per system, strategically placed near the times of quadrature, this integrates to 1.5×10^6 seconds, or nearly 54 8–hour nights of follow–up. This requirement highlights the interplay between the enormous discovery space enabled by wide–field surveys, and the commensurate demands on spectroscopic follow–up resources. We encourage the community to study these systems, and note that the many–orders–of–magnitude larger catalogs expected in the near future from time–domain surveys such as Pan–STARRS (Kaiser et al. 2002) and LSST (LSST Science Book 2009) will even further tax our limited abilities for spectroscopic follow–up.

ACKNOWLEDGMENTS

The authors thank Nicole Silvestri for useful discussions. A.C.B. acknowledges the support of NASA through grant NNX09AC77G. S.L.H. and A.F.K acknowledge the support of the NSF through grant AST 02-05875.

Funding for the SDSS and SDSS-II has been provided by the Alfred P. Sloan Foundation, the Participating Institutions, the National Science Foundation, the U.S. Department of Energy, the National Aeronautics and Space Administration, the Japanese Monbukagakusho, the Max Planck Society, and the Higher Education Funding Council for England. The SDSS Web Site is http://www.sdss.org/.

The SDSS is managed by the Astrophysical Research Consortium for the Participating Institutions. The Participating Institutions are the American Museum of Natural History, Astrophysical Institute Potsdam, University of Basel, University of Cambridge, Case Western Reserve University, University of Chicago, Drexel University, Fermilab, the Institute for Advanced Study, the Japan Participation Group, Johns Hopkins University, the Joint Institute for Nuclear Astrophysics, the Kavli Institute for Particle Astrophysics and Cosmology, the Korean Scientist Group, the Chinese Academy of Sciences (LAMOST), Los Alamos National Laboratory, the Max-Planck-Institute for Astronomy (MPIA), the Max-Planck-Institute for Astrophysics (MPA), New Mexico State University, Ohio State University, University of Pittsburgh, University of Portsmouth, Princeton University, the United States Naval Observatory, and the University of Washington.

REFERENCES

Abazajian, K. N., et al. 2009, ApJS, 182, 543
Anderson, S. F., et al. 2008, AJ, 135, 2108
Ankerst, M., Breunig, M. M., Kriegel, H.-P., & Sander, J. 1999, in SIGMOD 1999, Proceedings ACM SIGMOD International Conference on Management of Data, June 1-3, 1999, Philadephia, Pennsylvania, USA, ed. A. Delis, C. Faloutsos, & S. Ghandeharizadeh (ACM Press), 49–60
Artymowicz, P. & Lubow, S. H. 1994, ApJ, 421, 651
Baraffe, I., Chabrier, G., Allard, F., & Hauschildt, P. H. 1998, A&A, 337, 403
Becker, A. C., et al. 2008, MNRAS, 386, 416
Bhatti, W. A., Richmond, M. W., Ford, H. C., & Petro, L. D. 2010, ApJS, 186, 233
Blake, C. H., Torres, G., Bloom, J. S., & Gaudi, B. S. 2008, ApJ, 684, 635
Bochanski, J. J., et al. 2007a, AJ, 134, 2418
Bochanski, J. J., et al. 2007b, AJ, 133, 531
Bochanski, J. J. et al. 2010, AJ, 139, 2679
Bochanski, J. J. 2008, PhD thesis, University of Washington
Bond, N. A., et al. 2010, ApJ, 716, 1

Bramich, D. M., et al. 2008, MNRAS, 386, 887
Burrows, A., Hubbard, W. B., Saumon, D., & Lunine, J. I. 1993, ApJ, 406, 158
Chabrier, G., Gallardo, J., & Baraffe, I. 2007, A&A, 472, L17
Covey, K. R., et al. 2007, AJ, 134, 2398
Flannery, B. P. 1976, ApJ, 205, 217
Frieman, J. A., et al. 2008, AJ, 135, 338
Fukugita, M., et al. 1996, AJ, 111, 1748
Fuchs, B., et al. 2009, AJ, 137, 4149
Hawley, S. L. et al. 2002, AJ, 123, 3409
Hilton, E. J., West, A. A., Hawley, S. L., & Kowalski, A. F. 2010, AJ, 140, 1402
Howell, S. B., Nelson, L. A., & Rappaport, S. 2001, ApJ, 550, 897
Howell, S. B., Rappaport, S., & Politano, M. 1997, MNRAS, 287, 929
Ivezić, Ž., et al. 2008, ApJ, 684, 287
Ivezić, Ž., et al. 2007, AJ, 134, 973
Jurić, M., et al. 2008, ApJ, 673, 864
Kaib, N. A., et al. 2009, ApJ, 695, 268
Kaiser, N., et al. 2002, in Presented at the Society of Photo-Optical Instrumentation Engineers (SPIE) Conference, Vol. 4836, Society of Photo-Optical Instrumentation Engineers (SPIE) Conference Series, ed. J. A. Tyson & S. Wolff, 154–164
Kolb, U. 1993, A&A, 271, 149
Kowalski, A. F., et al. 2009, AJ, 138, 633
Kruse, E. A., et al. 2010, ApJ, 722, 1352
LSST Science Collaborations and LSST Project 2009, LSST Science Book, Version 2.0, arXiv:0912.0201, http://www.lsst.org/lsst/scibook
López-Morales, M. 2007, ApJ, 660, 732
Lucy, L. B. 1968, ApJ, 153, 877
Maceroni, C. & Rucinski, S. M. 1997, PASP, 109, 782
Marshall, D. J., et al. 2006, A&A, 453, 635
Mazeh, T. 2008, EAS Publications Series, 29, 1–65
Morales, J. C., et al. 2010, ApJ, 718, 502
Mullan, D. J. & MacDonald, J. 2001, ApJ, 559, 353
Nagel, T., et al. 2006, A&A, 448, L25
Oh, H.-S., Nychka, D., Brown, T., & Charbonneau, P. 2004, Journal Of The Royal Statistical Society Series C, 53, 15
Paczyński, B., Szczygieł, D. M., Pilecki, B., & Pojmański, G. 2006, MNRAS, 368, 1311
Perlmutter, S., et al. 1999, ApJ, 517, 565
Pojmanski, G. 2002, Acta Astronomica, 52, 397
Ribas, I. 2006, Ap&SS, 304, 89
Reimann, J. D. 1994, PhD thesis, “Frequency Estimation Using Unequally-Spaced Astronomical Data”, University of California, Berkeley
Riess, A. G., et al. 1998, AJ, 116, 1009
Rucinski, S. M. 1997, AJ, 113, 407
—. 2006, MNRAS, 368, 1319
—. 2007, MNRAS, 382, 393
Sako, M., et al. 2008, AJ, 135, 348
Schlegel, D. J., Finkbeiner, D. P., & Davis, M. 1998, ApJ, 500, 525
Schmidt, S. J., West, A. A., Hawley, S. L., & Pineda, J. S. 2010, AJ, 139, 1808
Sesar, B., et al. 2007, AJ, 134, 2236
Sesar, B., et al. 2010, ApJ, 708, 717
Shaw, J. S. & López-Morales, M. 2007, in Astronomical Society of the Pacific Conference Series, Vol. 362, The Seventh Pacific Rim Conference on Stellar Astrophysics, ed. Y. W. Kang, H.-W. Lee, K.-C. Leung, & K.-S. Cheng, 15–+
Silvestri, N. M., et al. 2006, AJ, 131, 1674
Skrutskie, M. F., et al. 2006, AJ, 131, 1163
Smolčić, V., et al. 2004, ApJ, 615, L141
Stepien, K. 2006, Acta Astronomica, 56, 347
Szkody, P., et al. 2003, ApJ, 583, 902
Szkody, P., Linnell, A. P., Campbell, R. K., Plotkin, R. M., Harrison, T. E., Holtzman, J., Seibert, M., & Howell, S. B. 2008, ApJ, 683, 967
Vidrih, S., et al. 2007, MNRAS, 382, 515
Watkins, L. L., et al. 2009, MNRAS, 398, 1757
West, A. A., et al. 2008, AJ, 135, 785
West, A. A., et al. 2004, AJ, 128, 426
West, A. A., Walkowicz, L. M., & Hawley, S. L. 2005, PASP, 117, 706
York, D. G., et al. 2000, AJ, 120, 1579

Table 1 Summary of the 207 periodic variables in SDSS Stripe 82. We list the mean r–band magnitude and mean colors of the system, de–reddened using the prescription of Schlegel et al. (1998). We provide our derived period for the system, defined such that the folded lightcurve has two maxima and minima. We also provide a quality estimate of the folded lightcurve, described in Section 3.

Name	r	$u-g$	$g-r$	$r-i$	$i-z$	**Period (days)**	**Quality**
SDSS J195954.01-002031.4	18.01	2.04	1.11	0.53	0.26	0.1975559	A
SDSS J200011.19+003806.5	17.28	1.79	1.31	1.37	0.72	0.1455201	B
SDSS J200022.52+010142.2	18.40	1.88	0.99	0.46	0.27	0.2250255	B
SDSS J200126.50-010932.7	17.71	1.79	0.89	0.40	0.18	0.2841651	B
SDSS J200215.36+001131.4	15.69	2.12	0.93	0.38	0.24	6.0435586	B
SDSS J200237.30+000335.4	17.62	2.13	1.24	0.66	0.37	0.9902033	B
SDSS J200352.35+003621.5	17.70	2.13	1.18	0.58	0.33	2.4448330	B
SDSS J200432.38+001041.3	19.34	1.18	0.96	0.39	0.20	0.2590820	B
SDSS J200526.79-003355.3	18.93	1.64	1.41	1.10	0.59	0.5333477	B
SDSS J200537.23-004700.7	18.92	0.95	1.06	0.73	0.44	0.3035355	B
SDSS J200733.65-003802.4	20.29	1.20	1.45	1.15	0.61	0.2866160	B
SDSS J200939.56+004111.2	16.38	2.37	1.08	0.43	0.22	0.2423517	A
SDSS J201031.94-010752.5	16.21	2.28	1.16	0.52	0.27	0.2682265	B
SDSS J201210.97-001437.5	18.71	1.92	0.87	0.42	0.21	0.2937543	C
SDSS J201316.07+004530.8	17.59	2.22	1.24	0.68	0.41	1.0106292	C
SDSS J201359.32-003536.5	19.20	1.32	0.94	0.40	0.20	0.2330079	B
SDSS J201532.52+010620.9	17.28	1.96	1.36	1.45	0.72	3.3104552	C
SDSS J201629.55-005837.7	17.88	1.95	1.06	0.43	0.24	0.2198742	A
SDSS J201920.65-010418.5	17.28	2.09	0.93	0.45	0.27	0.3779489	C
SDSS J202005.83-000153.6	19.07	1.64	1.03	0.43	0.26	0.2279430	B
SDSS J202054.31+011515.0	19.25	1.61	1.28	0.93	0.48	0.2585596	B
SDSS J202149.34+002125.3	18.75	1.84	1.02	0.44	0.24	0.2365252	B
SDSS J202247.66-002902.4	18.55	1.96	1.08	0.50	0.31	0.2352012	B
SDSS J202401.30+000910.2	14.90	2.15	1.05	0.41	0.20	0.2545827	A
SDSS J202428.40+004009.2	17.42	1.87	1.24	0.82	0.41	1.2406823	C
SDSS J202443.23-000729.2	18.51	1.82	1.15	0.63	0.42	1.2556512	C
SDSS J202445.58+001743.7	17.92	1.80	0.99	0.42	0.23	0.3062025	A
SDSS J202449.56-000729.3	16.12	2.06	0.95	0.39	0.24	0.8550228	B
SDSS J202510.30+004747.7	19.66	1.42	1.12	0.49	0.27	0.2355685	B

Continued on Next Page. . .

TABLE 1 – Continued

Name	r	$u-g$	$g-r$	$r-i$	$i-z$	**Period (days)**	**Quality**
SDSS J202518.82-010200.4	16.68	2.14	0.96	0.42	0.29	7.1900371	B
SDSS J202617.44-003738.6	18.56	1.87	1.36	0.79	0.46	0.2257140	B
SDSS J202651.76-003452.6	17.86	2.03	1.01	0.40	0.20	0.2190038	A
SDSS J202928.30-011327.8	18.82	1.55	0.94	0.33	0.18	0.2622347	B
SDSS J203240.64-011527.6	19.80	1.71	1.20	0.67	0.40	0.2854194	B
SDSS J203314.24-000523.1	17.78	2.15	1.32	0.62	0.34	0.3628127	A
SDSS J203400.96-000222.4	16.71	2.29	1.06	0.42	0.24	0.8461972	C
SDSS J203421.16+011013.2	19.22	1.79	0.99	0.48	0.26	0.6169044	B
SDSS J203454.94+002959.4	16.65	2.04	1.25	0.63	0.34	0.2883654	B
SDSS J203513.10-005239.2	18.95	1.68	1.03	0.51	0.31	0.4541513	C
SDSS J203521.96-011413.5	18.64	1.88	1.09	0.46	0.26	0.2225604	A
SDSS J203528.19+001908.1	20.27	0.84	0.68	1.34	0.76	0.3697745	C
SDSS J203940.39+001326.7	16.27	2.08	1.24	0.62	0.36	0.2376598	B
SDSS J204138.75+000835.4	19.67	1.32	1.11	0.64	0.41	0.9376321	B
SDSS J204218.17-005222.2	20.37	1.55	1.30	1.37	0.74	0.4097680	B
SDSS J204308.35-001153.3	17.06	2.38	1.11	0.51	0.28	0.2344230	A
SDSS J204323.64+000355.0	19.74	1.59	0.99	0.48	0.30	0.6359970	C
SDSS J204409.16-010355.6	18.93	2.08	1.22	0.52	0.29	0.2050373	B
SDSS J204427.38+000608.9	20.30	0.94	1.30	0.73	0.40	0.7156987	C
SDSS J204928.66-000945.3	18.58	1.92	0.95	0.48	0.29	0.7313443	B
SDSS J204959.44-005341.4	19.07	1.84	1.24	0.65	0.39	1.0175109	C
SDSS J205129.61+010656.4	19.13	1.73	1.36	0.61	0.34	0.4845315	B
SDSS J205321.73+001536.4	16.78	0.74	0.89	1.04	0.60	0.1789707	A
SDSS J205322.16-004918.9	19.29	1.75	1.30	1.06	0.58	0.8545925	C
SDSS J205329.31-001234.3	17.71	2.41	1.18	0.63	0.41	2.6139056	C
SDSS J205435.12+003300.9	18.53	2.05	1.34	1.17	0.64	0.3399066	C
SDSS J205438.11-005241.9	19.06	2.31	1.15	0.49	0.28	0.2321992	C
SDSS J205511.92-002309.3	20.03	1.51	1.43	1.31	0.69	0.2819485	B
SDSS J205632.59-005627.1	16.71	2.43	1.35	0.93	0.49	1.2392850	C
SDSS J205703.28+000945.9	18.83	1.83	0.93	0.47	0.28	0.2987312	C
SDSS J205814.56-010306.0	17.92	2.39	1.34	0.77	0.44	3.5761782	C
SDSS J205826.23-003202.4	18.12	2.19	1.29	0.53	0.29	0.9907401	C
SDSS J205836.60-001949.6	17.49	2.22	1.27	0.72	0.41	0.2129114	C
SDSS J210023.58-004204.1	16.89	2.43	1.16	0.51	0.30	0.7742631	C
SDSS J210302.06+001218.3	20.53	0.79	1.33	0.66	0.42	0.5113666	C
SDSS J210343.88+000303.2	16.44	1.66	1.26	1.01	0.58	0.2051351	C
SDSS J210454.18-004653.5	18.31	2.22	1.39	1.04	0.57	0.9508488	B
SDSS J210558.05-002420.9	18.63	1.92	1.18	0.61	0.38	0.5108677	B
SDSS J210616.41-003934.5	15.47	2.40	1.15	0.47	0.26	0.2237032	A
SDSS J210637.43+001249.8	20.24	1.03	1.19	0.61	0.38	0.2284199	A
SDSS J210726.81-003231.1	16.86	2.41	1.24	0.63	0.39	0.2540927	A
SDSS J210750.98-000011.8	15.79	2.33	1.27	0.72	0.41	0.4890171	B
SDSS J210803.61+001817.0	17.80	2.30	1.22	0.58	0.32	0.1799428	B
SDSS J210959.44+000054.9	18.16	2.13	1.19	0.60	0.38	0.7262478	C
SDSS J211314.48+000946.0	15.14	2.27	1.06	0.51	0.31	0.9566921	C
SDSS J211343.89+004544.3	18.50	1.90	1.31	0.99	0.53	0.5042300	C
SDSS J211428.41-010357.2	18.26	0.00	0.08	0.61	0.51	0.8211951	C
SDSS J211447.03-002902.1	19.38	1.87	1.27	0.81	0.47	0.2354735	C
SDSS J211529.11-001859.6	19.86	1.57	1.44	1.32	0.72	0.6589625	C
SDSS J211552.58+010820.5	20.39	0.72	1.32	1.33	0.70	0.4595826	C
SDSS J211710.61-003141.2	17.51	2.46	1.45	0.89	0.49	0.0723023	C
SDSS J211735.06+000744.4	17.50	2.32	1.41	0.94	0.52	0.1381198	C
SDSS J211752.59-001203.3	19.02	1.92	1.04	0.55	0.34	0.3087562	C
SDSS J212203.13-010053.3	17.41	2.46	1.30	0.73	0.45	0.7910802	B
SDSS J212257.90-003639.9	19.33	1.99	1.42	0.93	0.54	0.2226377	B
SDSS J212317.32+001452.8	19.85	1.56	1.43	1.09	0.59	0.8694058	C
SDSS J212323.18+001239.8	18.91	2.00	1.12	0.64	0.44	4.1407657	B
SDSS J212404.80+002456.9	18.70	2.02	1.37	0.82	0.46	0.8317383	B
SDSS J212404.88-000103.6	19.29	2.20	1.42	1.65	0.92	1.6968390	B
SDSS J212459.14+005441.1	19.60	1.16	1.40	1.51	0.80	2.1732331	B
SDSS J212531.92-010745.8	17.59	-0.45	-0.23	-0.07	-0.09	0.5796356	A
SDSS J212723.59-005210.8	17.00	2.26	1.44	1.56	0.85	0.7943670	B
SDSS J212806.16-001458.9	19.22	1.80	1.37	1.27	0.72	0.4491180	C
SDSS J212834.81+004127.6	17.94	1.93	1.45	1.55	0.85	0.7699017	B
SDSS J212923.44+005652.6	14.53	2.40	1.23	0.57	0.32	0.9478636	B
SDSS J213102.62+003132.6	18.96	1.79	0.97	0.48	0.31	0.6537385	C
SDSS J213113.99-005125.4	18.63	2.14	1.20	0.54	0.33	0.3490403	B
SDSS J213217.11-004923.2	16.70	2.47	1.24	0.65	0.39	0.3178997	B
SDSS J213604.35+010304.2	19.14	1.80	1.45	0.63	0.36	0.1421261	B
SDSS J213651.60+010245.5	19.26	1.92	1.13	0.56	0.39	1.3008586	B
SDSS J213804.17+001240.6	19.64	1.59	1.42	1.06	0.59	0.8985627	B
SDSS J214043.65-010713.0	18.73	-0.19	1.46	1.64	0.89	2.7627724	B
SDSS J214049.37+010814.0	17.69	2.31	1.16	0.55	0.31	0.6428419	B
SDSS J214109.00+011114.4	19.41	1.79	1.02	0.54	0.35	0.3958882	C
SDSS J214426.03+004517.0	17.09	2.32	1.19	0.54	0.29	0.2345329	A
SDSS J214439.75+011215.7	18.54	2.03	1.00	0.52	0.33	0.3094293	B

Continued on Next Page. . .

TABLE 1 – Continued

Name	r	$u-g$	$g-r$	$r-i$	$i-z$	**Period (days)**	**Quality**
SDSS J214559.50+005714.2	16.43	2.23	1.12	0.48	0.26	0.3949126	B
SDSS J214617.64+004536.1	20.13	1.31	1.41	0.91	0.50	0.5050460	B
SDSS J214758.26-001130.6	18.49	2.21	1.23	0.64	0.41	0.4132894	B
SDSS J214824.41+005847.1	16.81	2.28	1.26	0.79	0.44	0.8080211	C
SDSS J215136.74-001400.6	17.90	2.23	1.30	0.57	0.32	0.2349285	B
SDSS J215248.73-011012.1	18.98	1.51	1.48	1.53	0.82	1.3631094	C
SDSS J215258.38-005309.3	19.24	1.72	1.20	0.56	0.32	0.2328584	B
SDSS J215802.85+002643.3	18.59	2.09	1.27	0.68	0.39	0.6656878	C
SDSS J215811.08+002246.9	15.15	2.14	1.02	0.48	0.28	0.4949717	C
SDSS J215934.50+005652.7	19.36	1.71	0.93	0.47	0.30	0.6059072	B
SDSS J222234.92-001655.0	19.42	1.66	1.46	1.39	0.74	4.2820836	B
SDSS J222348.84-005332.6	18.33	2.18	1.06	0.54	0.33	0.2880042	B
SDSS J223019.23-001155.1	17.67	2.34	1.32	0.67	0.39	0.3691831	B
SDSS J224718.54+001741.0	17.17	2.27	1.43	0.83	0.46	0.2697419	B
SDSS J224836.22+005707.6	17.82	2.18	1.38	1.11	0.61	2.4625131	B
SDSS J230032.79-002318.0	20.04	1.32	1.37	0.93	0.53	0.2866570	B
SDSS J230037.41+003159.7	19.20	1.88	1.49	1.03	0.56	0.3844287	C
SDSS J230039.13+004952.7	18.79	1.63	1.37	1.40	0.80	0.7852108	C
SDSS J230134.00-001912.0	15.99	2.37	1.14	0.49	0.29	0.5526236	B
SDSS J230257.39+005011.4	19.64	1.69	1.38	0.81	0.48	0.3594605	C
SDSS J230524.26+004746.8	18.42	2.17	1.26	0.64	0.36	0.6843911	C
SDSS J230608.92+001142.3	18.65	2.09	1.26	0.70	0.43	2.1694002	C
SDSS J230713.29-011437.1	20.24	0.02	0.32	0.00	0.16	0.6659821	C
SDSS J230939.86+010417.0	16.40	2.23	1.38	1.04	0.58	1.5547550	B
SDSS J231437.24-011212.8	15.31	2.41	1.19	0.59	0.36	1.2260650	B
SDSS J231611.41+005151.1	17.01	2.17	1.41	1.44	0.77	0.9049369	B
SDSS J231823.93-004415.2	19.15	1.98	1.29	0.74	0.42	0.2175166	B
SDSS J231901.29+000319.2	17.84	2.32	1.24	0.62	0.40	0.3300759	C
SDSS J232055.10+002745.3	16.90	1.86	1.39	1.19	0.66	0.2353853	B
SDSS J232122.34-001928.7	18.14	2.24	1.16	0.50	0.28	0.5190213	B
SDSS J232326.66+000309.9	18.96	2.02	1.25	0.64	0.39	0.5951980	B
SDSS J232641.19+004744.1	15.62	2.13	0.97	0.50	0.33	0.7668645	B
SDSS J233408.77+002704.4	19.12	1.96	1.42	0.84	0.47	0.2355482	B
SDSS J233538.33-002927.3	19.07	1.25	1.52	1.81	1.04	0.9763013	B
SDSS J234309.23-005717.1	20.17	1.58	1.40	1.35	0.76	1.1236505	B
SDSS J234541.84+002621.1	19.07	1.67	1.48	0.68	0.39	0.3930952	B
SDSS J234809.83-003156.4	17.16	2.48	1.36	0.68	0.40	0.4207058	B
SDSS J235320.34+001614.1	18.28	2.03	1.44	1.42	0.78	0.9562803	B
SDSS J235540.00-000343.0	18.59	2.15	1.34	0.95	0.53	0.4870803	B
SDSS J000308.69+000749.0	18.55	2.25	1.44	1.33	0.72	2.2890031	B
SDSS J000436.67+010537.6	19.53	1.36	1.34	1.33	0.74	0.9291190	B
SDSS J000753.50+001759.7	17.63	2.31	1.40	1.01	0.58	0.4243976	A
SDSS J000906.42-000753.1	19.12	1.96	1.47	0.89	0.49	0.7608881	B
SDSS J001641.03-000925.2	16.36	2.55	1.33	0.64	0.34	0.1985615	B
SDSS J002836.99-004514.9	15.11	2.41	1.20	0.59	0.35	0.2579071	A
SDSS J003023.53+001432.7	17.39	2.25	1.41	1.34	0.72	1.3186429	C
SDSS J003034.05+003916.9	17.70	2.06	0.99	0.50	0.30	0.3197141	C
SDSS J003042.11+003420.1	19.10	1.95	1.50	1.14	0.63	0.3718388	B
SDSS J003316.30-001752.2	16.56	2.44	1.44	1.30	0.70	1.1820390	B
SDSS J003322.03-005552.6	17.60	2.45	1.37	0.79	0.45	0.8624634	B
SDSS J003628.06-003124.8	19.22	0.03	0.02	0.66	0.60	0.4096298	B
SDSS J003841.29+010756.0	17.49	2.33	1.31	0.79	0.49	2.7614820	C
SDSS J005506.78-005702.4	16.22	2.29	1.39	1.33	0.75	0.2524701	B
SDSS J005705.17+000704.7	19.06	1.81	1.37	1.40	0.76	0.8858173	C
SDSS J005841.71+011337.8	18.40	2.22	1.38	0.71	0.40	0.6555093	B
SDSS J012119.10-001949.9	15.50	2.49	1.22	0.51	0.27	0.2072812	A
SDSS J013125.14-011100.1	18.51	2.25	1.50	1.29	0.70	0.6207617	B
SDSS J013155.94-004224.7	16.34	2.70	1.55	1.83	1.02	0.3511764	C
SDSS J013851.54-001621.6	17.43	1.71	1.41	1.77	1.00	0.0727650	B
SDSS J015940.00+010328.4	20.04	1.48	1.43	0.67	0.41	0.3377942	B
SDSS J020448.41+011052.2	15.77	2.21	1.35	0.78	0.43	0.3188949	B
SDSS J021121.56-003808.3	17.79	2.39	1.32	0.71	0.43	0.6236612	B
SDSS J022548.47+004907.1	17.18	2.24	1.11	0.50	0.30	1.5676510	B
SDSS J023614.59-002814.4	19.13	1.86	1.46	1.33	0.74	0.8038365	C
SDSS J023857.17-000428.9	18.69	2.27	1.36	0.99	0.53	0.2804496	C
SDSS J024013.79-003759.7	18.68	2.20	1.21	0.65	0.41	0.3457496	C
SDSS J024053.10+005944.9	18.66	2.25	1.24	0.56	0.32	0.4839048	B
SDSS J024319.19-010218.1	18.70	2.08	1.45	1.51	0.84	3.8409523	B
SDSS J024446.51+003653.2	18.25	2.15	1.05	0.51	0.33	0.2968753	B
SDSS J024835.93+010520.2	18.73	2.00	1.42	1.31	0.72	0.8475098	C
SDSS J024843.68-010055.3	18.23	2.31	1.32	0.63	0.36	1.1436785	C
SDSS J025331.12-000226.0	19.34	1.86	1.32	0.89	0.48	1.1706181	C
SDSS J025403.75+005854.2	17.42	-0.54	-0.61	-0.42	-0.37	2.1744163	A
SDSS J025828.09+004758.7	17.99	2.15	1.43	0.89	0.50	0.4856080	B
SDSS J025953.33-004400.2	19.29	0.73	1.18	1.05	0.71	0.1441834	B
SDSS J030304.48+004809.4	16.99	2.30	1.25	0.64	0.41	0.4412123	C

Continued on Next Page. . .

TABLE 1 – Continued

Name	r	$u-g$	$g-r$	$r-i$	$i-z$	**Period (days)**	**Quality**
SDSS J030402.15+004551.4	16.66	1.51	1.43	2.03	1.13	2.5850529	B
SDSS J030834.42+005835.2	19.47	1.91	1.12	0.47	0.27	0.2708025	B
SDSS J030856.55-005450.7	17.42	1.56	1.20	1.24	0.69	0.1859601	A
SDSS J031151.73-000123.6	18.90	2.02	1.32	1.19	0.66	1.1066820	C
SDSS J031442.23+001030.3	17.89	1.79	1.26	0.61	0.34	0.2365776	B
SDSS J031708.46-005846.1	17.49	2.41	1.39	0.72	0.41	1.0233606	B
SDSS J031820.88-003131.0	17.25	2.38	1.42	0.98	0.57	0.6381190	C
SDSS J031858.28+002325.6	18.65	-0.55	-0.60	-0.41	-0.34	7.0480973	B
SDSS J032048.68+003234.0	16.19	2.05	1.01	0.48	0.28	1.4682549	C
SDSS J032325.85+010634.9	15.57	2.27	1.33	0.64	0.36	0.3297024	B
SDSS J032413.10+000441.7	18.72	1.89	1.24	0.56	0.30	0.3066937	B
SDSS J032515.05-010239.7	18.43	2.18	1.46	1.00	0.56	0.3945195	C
SDSS J032949.17-001240.8	19.77	1.38	1.36	0.58	0.36	0.3919553	B
SDSS J033031.37-000137.5	15.35	2.33	1.33	1.42	0.75	1.6782523	C
SDSS J033513.80+004252.8	18.82	0.63	0.92	0.67	0.40	0.5473870	B
SDSS J033606.30+004959.4	16.98	2.32	1.23	0.58	0.37	0.3383779	C
SDSS J034302.81+010935.6	14.49	2.00	0.94	0.39	0.21	0.6119363	B
SDSS J034748.36+002604.6	18.21	1.78	1.44	0.87	0.45	1.0726766	B
SDSS J035003.61+000311.4	18.51	1.51	1.25	0.91	0.53	0.2407845	B
SDSS J035300.50+004835.9	19.30	1.30	1.30	1.13	0.60	0.1605031	B
SDSS J035325.66+000220.3	15.01	2.09	1.06	0.53	0.27	0.8541573	C
SDSS J035856.16+004010.2	18.06	1.42	0.75	0.30	0.12	0.2246616	B
SDSS J040034.93-003816.2	14.07	2.00	0.88	0.33	0.15	0.2561826	A
SDSS J040054.13+005743.8	19.32	0.75	0.62	0.27	0.08	0.2147133	C
SDSS J040104.52-004409.8	13.89	1.93	0.84	0.39	0.17	0.7604045	C
SDSS J040111.09-002959.1	18.46	1.37	1.03	0.41	0.22	0.3500603	C

Table 2 System classifications for all 207 of our periodic objects. Mean colors are used to estimate a **Color**–based classification using the M–dwarf color–spectral type relationships of Kowalski et al. (2009). Systems with $u - g < 1.8$ also likely contain a white dwarf (WD). Twenty–nine of the systems have spectra available from SDSS, and are used to make a **Spectral** classification using the software of Covey et al. (2007). Finally, we use the folded lightcurve shape–based methods of Pojmanski (2002) and Rucinski (1997) to constrain the geometry of the system using the g, r, and i–band data. This **Binary Class** may be eclipsing (EC, EC^{*}), semi–detached (ESD), or detached (ED, ED^{*}). We have highest confidence in the classification of those systems where **Binary Class**$_g$ = **Binary Class**$_r$ = **Binary Class**$_i$, which represent the subset of systems used in the analysis of Section 5.

Name	**Color Class**	**Spectral Class**	**Binary Class**$_g$	**Binary Class**$_r$	**Binary Class**$_i$
SDSS J195954.01-002031.4	M1	···	EC*	EC*	ESD
SDSS J200011.19+003806.5	M4	···	EC*	EC*	EC*
SDSS J200022.52+010142.2	M0	···	EC	ESD	EC
SDSS J200126.50-010932.7	M0	···	EC	ESD	ESD
SDSS J200215.36+001131.4	M0	···	ESD	ESD	ESD
SDSS J200237.30+000335.4	M1	···	EC	EC	EC
SDSS J200352.35+003621.5	M3	···	EC/ESD	EC	ESD
SDSS J200432.38+001041.3	M0+WD	···	EC*	EC*	EC*
SDSS J200526.79-003355.3	M3	···	EC	ED	ED*
SDSS J200537.23-004700.7	M1+WD	···	EC*	ESD	ESD
SDSS J200733.65-003802.4	M3+WD	···	ED	ESD/ED	ED
SDSS J200939.56+004111.2	M0	···	EC*	EC	EC
SDSS J201031.94-010752.5	M1	···	EC	EC	EC
SDSS J201210.97-001437.5	M0	···	EC	EC	ESD
SDSS J201316.07+004530.8	M2	···	ESD	ESD	ESD
SDSS J201359.32-003536.5	M0+WD	···	EC*	EC	EC
SDSS J201532.52+010620.9	M4	···	EC	EC	EC
SDSS J201629.55-005837.7	M0	···	EC	EC*	EC
SDSS J201920.65-010418.5	M0	···	ED*	ED	ED
SDSS J202005.83-000153.6	M0	···	EC	EC	ESD
SDSS J202054.31+011515.0	M2	···	ESD	ED	ED
SDSS J202149.34+002125.3	M0	···	EC	EC*	EC
SDSS J202247.66-002902.4	M0	···	EC	EC	EC
SDSS J202401.30+000910.2	M0	···	EC*	ED*	EC*
SDSS J202428.40+004009.2	M2	···	ESD	ESD	ESD
SDSS J202443.23-000729.2	M1	···	EC	EC/ESD	EC/ESD
SDSS J202445.58+001743.7	M0	···	ESD	ESD	ESD
SDSS J202449.56-000729.3	M0	···	ED	ED*	ED
SDSS J202510.30+004747.7	M1+WD	···	EC*	EC	EC
SDSS J202518.82-010200.4	M0	···	EC	EC*	EC
SDSS J202617.44-003738.6	M2	···	EC	EC	EC
SDSS J202651.76-003452.6	M0	···	EC*	EC*	EC*
SDSS J202928.30-011327.8	M0	···	EC	EC	EC
SDSS J203240.64-011527.6	M1	···	EC	ESD	ESD
SDSS J203314.24-000523.1	M2	···	ED	ED	ED
SDSS J203400.96-000222.4	M0	···	EC	EC/ESD	EC
SDSS J203421.16+011013.2	M0	···	ED	ED	ED
SDSS J203454.94+002959.4	M2	···	ESD	EC/ESD	ESD
SDSS J203513.10-005239.2	M1	···	ED*	ED	ED
SDSS J203521.96-011413.5	M0	···	EC*	EC*	EC*
SDSS J203528.19+001908.1	M4+WD	···	EC*	ED*	ED*
SDSS J203940.39+001326.7	M1	···	EC*	EC*	EC*
SDSS J204138.75+000835.4	M1+WD	···	ESD	ESD	ESD
SDSS J204218.17-005222.2	M4+WD	···	ED	ED*	ED
SDSS J204308.35-001153.3	M0	···	EC*	EC*	EC
SDSS J204323.64+000355.0	M0+WD	···	ED*	ED*	ED*
SDSS J204409.16-010355.6	M0	···	EC	EC	EC
SDSS J204427.38+000608.9	M2+WD	···	ESD	ED	ESD/ED
SDSS J204928.66-000945.3	M0	···	ED*	ED*	ED*
SDSS J204959.44-005341.4	M1	···	ED*	ED*	ED*
SDSS J205129.61+010656.4	M1	···	ED	ED	ED
SDSS J205321.73+001536.4	M3+WD	···	EC/ESD	EC	EC
SDSS J205322.16-004918.9	M3	···	ED	ED*	ED*
SDSS J205329.31-001234.3	M2	···	ESD	ESD	EC*
SDSS J205435.12+003300.9	M3	···	ESD/ED	ESD	ESD
SDSS J205438.11-005241.9	M0	···	ESD	EC	EC
SDSS J205511.92-002309.3	M4+WD	···	ESD/ED	ED	ED*
SDSS J205632.59-005627.1	M2	···	ESD/ED	ESD	ESD/ED
SDSS J205703.28+000945.9	M0	···	ESD	ESD	ESD
SDSS J205814.56-010306.0	M2	···	ESD	ESD	EC/ESD
SDSS J205826.23-003202.4	M1	···	ED*	ED	ED
SDSS J205836.60-001949.6	M2	···	EC	EC/ESD	EC/ESD
SDSS J210023.58-004204.1	M0	···	EC*	EC*	EC*
SDSS J210302.06+001218.3	M1+WD	···	ED*	ED	ED

Continued on Next Page…

TABLE 2 – Continued

Name	**Color Class**	**Spectral Class**	**Binary Class$_g$**	**Binary Class$_r$**	**Binary Class$_i$**
SDSS J210343.88+000303.2	M2+WD	···	EC	EC	ESD
SDSS J210454.18-004653.5	M2	···	ED*	ED	ED
SDSS J210558.05-002420.9	M1	···	ED	ED	ED
SDSS J210616.41-003934.5	M0	···	EC	EC	EC
SDSS J210637.43+001249.8	M1+WD	···	EC*	EC	EC
SDSS J210726.81-003231.1	M1	···	EC	EC	EC
SDSS J210750.98-000011.8	M2	···	ED	ED	ED
SDSS J210803.61+001817.0	M1	···	EC	EC	EC/ESD
SDSS J210959.44+000054.9	M2	···	ED	ED	ED
SDSS J211314.48+000946.0	M1	···	ESD/ED	ED	ED
SDSS J211343.89+004544.3	M3	···	ESD/ED	ESD	ESD/ED
SDSS J211428.41-010357.2	M1+WD	M+WD	EC*	EC	EC/ESD
SDSS J211447.03-002902.1	M1	···	ESD	ESD	ESD/ED
SDSS J211529.11-001859.6	M4+WD	···	ESD	ED	ED
SDSS J211552.58+010820.5	M4+WD	···	ED*	ED	ED
SDSS J211710.61-003141.2	M2	···	ED*	ED	ED
SDSS J211735.06+000744.4	M2	···	ED	ED*	ED
SDSS J211752.59-001203.3	M1	···	ESD	ESD	ESD
SDSS J212203.13-010053.3	M1	···	ED*	ED*	ED
SDSS J212257.90-003639.9	M2	···	ESD	ED*	ED*
SDSS J212317.32+001452.8	M3+WD	···	ED*	ED*	ED*
SDSS J212323.18+001239.8	M1	···	EC	EC	ESD
SDSS J212404.80+002456.9	M2	···	ED	ED*	ED
SDSS J212404.88-000103.6	M5	···	ESD/ED	ESD/ED	ESD
SDSS J212459.14+005441.1	M4+WD	···	EC	EC	ESD
SDSS J212531.92-010745.8	WD	WD	EC*	EC*	EC*
SDSS J212723.59-005210.8	M4	···	EC/ESD	EC/ESD	ESD/ED
SDSS J212806.16-001458.9	M4	···	ED	ED	ED
SDSS J212834.81+004127.6	M4	···	ESD	ESD	ESD
SDSS J212923.44+005652.6	M1	···	ED*	ED*	ED*
SDSS J213102.62+003132.6	M0	···	ED	ESD/ED	ED
SDSS J213113.99-005125.4	M0	···	ED	ED	ED
SDSS J213217.11-004923.2	M1	···	EC	ESD	ESD
SDSS J213604.35+010304.2	M1	···	ESD	ED	ED
SDSS J213651.60+010245.5	M0	···	ED*	ED*	ED*
SDSS J213804.17+001240.6	M3+WD	···	ED*	ED*	ED*
SDSS J214043.65-010713.0	M5+WD	···	EC*	EC	EC/ESD
SDSS J214049.37+010814.0	M1	···	ED*	ED	ED
SDSS J214109.00+011114.4	M0	···	ED	ED	ED
SDSS J214426.03+004517.0	M1	···	EC	EC	EC
SDSS J214439.75+011215.7	M0	···	ESD	ESD/ED	ESD
SDSS J214559.50+005714.2	M0	···	ED	ED	ED
SDSS J214617.64+004536.1	M2+WD	···	ED	ED	ED
SDSS J214758.26-001130.6	M2	···	ESD	ESD	ESD/ED
SDSS J214824.41+005847.1	M1	···	ED	ED	ED*
SDSS J215136.74-001400.6	M2	···	ESD/ED	ESD/ED	ED
SDSS J215248.73-011012.1	M5+WD	···	EC/ESD	EC	EC/ESD
SDSS J215258.38-005309.3	M1	···	EC	EC	EC
SDSS J215802.85+002643.3	M1	···	ED	ED	ED
SDSS J215811.08+002246.9	M0	···	ESD	ED	ED
SDSS J215934.50+005652.7	M0+WD	K5	ED	ED	ED
SDSS J222234.92-001655.0	M4+WD	···	ESD	ESD	EC/ESD
SDSS J222348.84-005332.6	M0	···	ESD	ESD	ESD
SDSS J223019.23-001155.1	M1	···	ED	ESD	ESD/ED
SDSS J224718.54+001741.0	M2	···	ESD	ESD/ED	EC/ESD
SDSS J224836.22+005707.6	M3	···	EC	EC	EC/ESD
SDSS J230032.79-002318.0	M2+WD	···	ESD	ESD	ED
SDSS J230037.41+003159.7	M2	···	ED	ED	ED
SDSS J230039.13+004952.7	M4+WD	···	ED	ESD/ED	ESD
SDSS J230134.00-001912.0	M0	···	ED	ED	ED
SDSS J230257.39+005011.4	M1+WD	···	ED	ED	ED
SDSS J230524.26+004746.8	M1	···	ED*	ED*	ED*
SDSS J230608.92+001142.3	M1	···	EC	ESD	ESD
SDSS J230713.29-011437.1	WD	···	EC*	EC*	EC*
SDSS J230939.86+010417.0	M2	···	ED	ED	ED
SDSS J231437.24-011212.8	M1	···	ESD	EC/ESD	EC/ESD
SDSS J231611.41+005151.1	M4	···	ESD	ESD	ESD/ED
SDSS J231823.93-004415.2	M1	···	EC	EC	EC
SDSS J231901.29+000319.2	M1	···	ESD	ESD	ESD
SDSS J232055.10+002745.3	M3	···	ESD	EC	EC
SDSS J232122.34-001928.7	M0	···	ESD/ED	ED	ED
SDSS J232326.66+000309.9	M1	···	ED	ED	ED
SDSS J232641.19+004744.1	M0	···	ESD	ESD	ESD
SDSS J233408.77+002704.4	M2	···	ESD	ESD	ESD
SDSS J233538.33-002927.3	M5+WD	···	EC	EC	EC*
SDSS J234309.23-005717.1	M4+WD	···	EC*	EC*	EC*

Continued on Next Page…

TABLE 2 – Continued

Name	**Color Class**	**Spectral Class**	**Binary Class$_g$**	**Binary Class$_r$**	**Binary Class$_i$**
SDSS J234541.84+002621.1	M1+WD	M1	ED	ED	ED
SDSS J234809.83-003156.4	M1	···	ED	ED	ESD/ED
SDSS J235320.34+001614.1	M4	M4	ESD/ED	EC	ESD
SDSS J235540.00-000343.0	M2	···	ED	ED	ED
SDSS J000308.69+000749.0	M4	···	EC	ESD	ESD
SDSS J000436.67+010537.6	M4+WD	···	ED	ESD	ED
SDSS J000753.50+001759.7	M2	M2	ED	ED	ED
SDSS J000906.42-000753.1	M2	···	ED	ED	ED
SDSS J001641.03-000925.2	M1	M0	EC	EC	EC
SDSS J002836.99-004514.9	M0	···	EC	EC	EC
SDSS J003023.53+001432.7	M4	M4	ED	ESD/ED	ESD/ED
SDSS J003034.05+003916.9	M0	···	ESD	ESD	ESD/ED
SDSS J003042.11+003420.1	M3	M4	ESD	ED	ED
SDSS J003316.30-001752.2	M4	M4	ESD/ED	ESD	ESD/ED
SDSS J003322.03-005552.6	M1	M1	ED*	ED*	ED*
SDSS J003628.06-003124.8	M1+WD	M+WD	ESD/ED	EC/ESD	EC/ESD
SDSS J003841.29+010756.0	M1	M1	ED*	ED*	ED*
SDSS J005506.78-005702.4	M4	M4	ESD	ED	ED
SDSS J005705.17+000704.7	M4	···	ED	ED	ED
SDSS J005841.71+011337.8	M1	···	ED	ED	ED*
SDSS J012119.10-001949.9	M0	M0	EC*	EC*	EC
SDSS J013125.14-011100.1	M4	···	ED*	ED*	ED*
SDSS J013155.94-004224.7	M5	···	ED	ED	ED
SDSS J013851.54-001621.6	M5+WD	M5	EC	EC	EC
SDSS J015940.00+010328.4	M0	···	ED	ED	ED
SDSS J020448.41+011052.2	M1	···	ESD	ESD	ESD
SDSS J021121.56-003808.3	M1	···	ED	ED	ED
SDSS J022548.47+004907.1	M0	M0	ED	ED	ED
SDSS J023614.59-002814.4	M4	···	ED*	ED	ED*
SDSS J023857.17-000428.9	M2	···	ESD/ED	ESD/ED	ED
SDSS J024013.79-003759.7	M1	···	ESD/ED	ESD/ED	ESD/ED
SDSS J024053.10+005944.9	M0	M0	ED	ESD/ED	ED
SDSS J024319.19-010218.1	M4	···	ESD	ESD	ESD
SDSS J024446.51+003653.2	M0	···	ESD	ESD	ESD
SDSS J024835.93+010520.2	M4	···	ED*	ED*	ED*
SDSS J024843.68-010055.3	M1	···	ED	ED*	ED*
SDSS J025331.12-000226.0	M2	M2	ED	ED*	ED
SDSS J025403.75+005854.2	WD	WD	EC*	EC*	EC*
SDSS J025828.09+004758.7	M2	···	ED	ED	ED
SDSS J025953.33-004400.2	M3+WD	M4	EC*	EC	EC
SDSS J030304.48+004809.4	M1	M1	ED	ED	ED
SDSS J030402.15+004551.4	M6+WD	M7	EC*	EC	ESD
SDSS J030834.42+005835.2	M0	···	ESD	ESD	ESD
SDSS J030856.55-005450.7	M4+WD	M4	EC	EC	EC
SDSS J031151.73-000123.6	M3	M4	ED*	ED*	ED*
SDSS J031442.23+001030.3	M1	···	EC	EC	EC
SDSS J031708.46-005846.1	M1	···	ED	ED*	ED*
SDSS J031820.88-003131.0	M2	···	ED	ED	ED
SDSS J031858.28+002325.6	WD	WD	EC/ESD	EC/ESD	EC/ESD
SDSS J032048.68+003234.0	M0	···	ED*	ED	ED*
SDSS J032325.85+010634.9	M2	···	ESD	ED	ED
SDSS J032413.10+000441.7	M1	···	ESD	ESD	ESD
SDSS J032515.05-010239.7	M2	M3	ED	ED	ED
SDSS J032949.17-001240.8	M1+WD	M0	ED	ED	ED*
SDSS J033031.37-000137.5	M4	···	EC/ESD	ESD	ESD
SDSS J033513.80+004252.8	M2+WD	M1+WD	EC/ESD	EC/ESD	EC/ESD
SDSS J033606.30+004959.4	M1	···	ESD	ESD	ESD
SDSS J034302.81+010935.6	M0	···	ED	ED	ED
SDSS J034748.36+002604.6	M2	···	ED*	ED*	ED
SDSS J035003.61+000311.4	M3	···	EC	EC	EC/ESD
SDSS J035300.50+004835.9	M4+WD	···	EC	EC	EC
SDSS J035325.66+000220.3	M3	···	ED	ED	ED*
SDSS J035856.16+004010.2	M4	···	EC	EC	EC
SDSS J040034.93-003816.2	M4	···	EC	EC	EC
SDSS J040054.13+005743.8	M3+WD	···	EC	ESD	ED*
SDSS J040104.52-004409.8	M4	···	ESD/ED	ESD	ESD
SDSS J040111.09-002959.1	M4	···	ED*	ED	ED

Table 3

Comparison of periodic objects found in SDSS Stripe 82 by Bhatti et al. (2010). We have run our pipeline on all 32 objects found in their catalog, 11 of which pass our color cuts. We fail to find a significant period for 5 of the objects, and disagree with their period on 4 of them (see Figure 1). We list the period ratios between the two studies; integer ratios represent period aliases, which we consider concordance between the studies.

Name	Period of Bhatti et al. (2010)	Period (days)	Period ratio
Objects passing our color cuts			
SDSS J002851.08+000751.0	0.59098	···	···
SDSS J003042.11+003420.1	0.45705	0.3718388	1:0.8
SDSS J015429.30+005326.7	2.63902	···	···
SDSS J015940.00+010328.4	0.33779	0.3377942	1:1.0
SDSS J021121.56-003808.3	0.31210	0.6236612	1:2.0
SDSS J025953.33-004400.2	0.14418	0.1441834	1:1.0
SDSS J030834.42+005835.2	0.27080	0.2708026	1:1.0
SDSS J031823.88-010018.4	0.40704	···	···
SDSS J032515.05-010239.7	0.39451	0.3945195	1:1.0
SDSS J032949.17-001240.8	0.39196	0.3919552	1:1.0
SDSS J035300.50+004835.9	0.14855	0.1605031	1:1.1
Objects not passing our color cuts			
SDSS J000845.39+002744.2	0.34419	0.4157259	1:1.2
SDSS J002719.16+002400.6	1.31839	···	···
SDSS J011155.73-002633.0	0.22758	0.2276482	1:1.0
SDSS J011156.52-005221.4	0.23002	0.2300215	1:1.0
SDSS J011302.57+004822.9	0.31660	1.2782116	1:4.0
SDSS J011405.02+001138.5	0.28550	0.2855018	1:1.0
SDSS J013536.05-011058.7	0.39226	0.3922680	1:1.0
SDSS J020540.08-002227.6	0.79789	0.7978849	1:1.0
SDSS J020816.51+003510.0	1.61420	1.6142439	1:1.0
SDSS J021624.34-001817.7	0.63678	0.6367674	1:1.0
SDSS J022733.94+002615.2	0.70626	0.7062323	1:1.0
SDSS J022858.99-004120.4	0.64725	···	···
SDSS J023621.96+011359.1	0.35666	0.3025580	1:0.8
SDSS J024109.55+004813.6	0.27645	0.2764460	1:1.0
SDSS J024255.78-001551.5	3.19764	3.1974704	1:1.0
SDSS J030753.52+005013.0	0.35353	0.3535264	1:1.0
SDSS J031002.47-000916.2	2.19058	2.1906948	1:1.0
SDSS J031021.22+001453.9	0.26684	0.2668447	1:1.0
SDSS J034256.26-000058.0	0.32034	0.3203364	1:1.0
SDSS J034757.70-001423.5	0.27509	0.2750874	1:1.0
SDSS J035138.50-003924.5	0.19892	0.1989188	1:1.0